

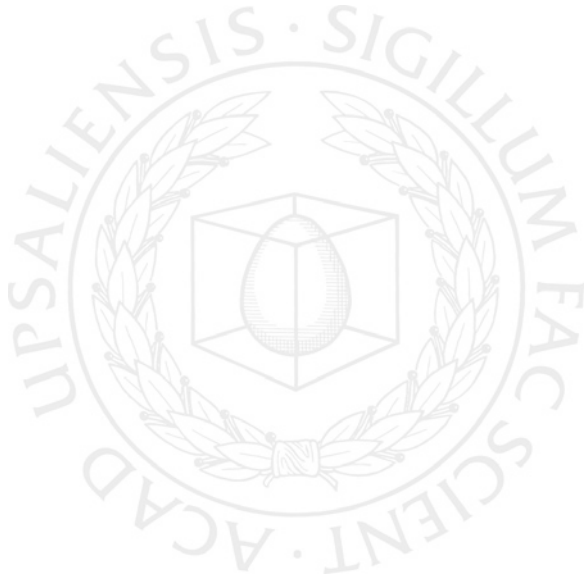


UPPSALA
UNIVERSITET

*Digital Comprehensive Summaries of Uppsala Dissertations
from the Faculty of Science and Technology 709*

Shape Optimization for Acoustic Wave Propagation Problems

RAJITHA UDAWALPOLA



ACTA
UNIVERSITATIS
UPSALIENSIS
UPPSALA
2010

ISSN 1651-6214
ISBN 978-91-554-7707-3
urn:nbn:se:uu:diva-112549

Dissertation presented at Uppsala University to be publicly examined in room 2446, building 2, Polacksbacken, Uppsala, Friday, February 26, 2010 at 10:15 for the degree of Doctor of Philosophy. The examination will be conducted in English

Abstract

Udawalpola, R. 2010. Shape Optimization for Acoustic Wave Propagation Problems. Acta Universitatis Upsaliensis. *Digital Comprehensive Summaries of Uppsala Dissertations from the Faculty of Science and Technology* 709. 42 pp. Uppsala. ISBN 978-91-554-7707-3

Boundary shape optimization is a technique to search for an optimal shape by modifying the boundary of a device with a pre-specified topology. We consider boundary shape optimization of acoustic horns in loudspeakers and brass wind instruments. A horn is an interfacial device, situated between a source, such as a waveguide or a transducer, and surrounding space. Horns are used to control both the transmission properties from the source and the spatial power distribution in the far-field (directivity patterns).

Transmission and directivity properties of a horn are sensitive to the shape of the horn flare. By changing the horn flare we design transmission efficient horns. However, it is difficult to achieve both controllability of directivity patterns and high transmission efficiency by using only changes in the horn flare. Therefore we use simultaneous shape and so-called topology optimization to design a horn/acoustic-lens combination to achieve high transmission efficiency and even directivity. We also design transmission efficient interfacial devices without imposing an upper constraint on the mouth diameter. The results demonstrate that there appears to be a natural limit on the optimal mouth diameter.

We optimize brass-wind instruments with respect to its intonation properties. The instrument is modeled using a hybrid method between a one-dimensional transmission line analogy for the slowly flaring part of the instrument, and a finite element model for the rapidly flaring part.

An experimental study is carried out to verify the transmission properties of an optimized horn. We produce a prototype of an optimized horn and then measure the input impedance of the horn. The measured values agree reasonably well with the predicted optimal values.

The finite element method and the boundary element method are used as discretization methods in the thesis. Gradient-based optimization methods are used for optimization, in which the gradients are supplied by the adjoint methods.

Keywords: Shape Optimization, Design Optimization, Acoustic wave propagation, Helmholtz Equation, The Boundary Element Method, The Finite Element Method, Inverse Problems, Adjoint Method, Gradient-based optimization

Rajitha Udawalpola, Department of Information Technology, Uppsala University, Box 337 SE-751 05 Uppsala, Sweden

© Rajitha Udawalpola 2010

ISSN 1651-6214

ISBN 978-91-554-7707-3

urn:nbn:se:uu:diva-112549 (<http://urn.kb.se/resolve?urn=urn:nbn:se:uu:diva-112549>)

To my late sister Anusha...

List of Papers

This thesis is based on the following papers, which are referred to in the text by their Roman numerals.

- I Udawalpola R., Berggren M. (2008) Optimization of an acoustic horn with respect to efficiency and directivity. *Int. J. Numer. Meth. Engng.*, 73(11):1571-1606, doi:10.1002/nme.2132.
Contributions: Implemented the method and performed all numerical experiments. Development of the method and preparation of the manuscript was done in close cooperation with the co-author.
- II Wadbro E., Udawalpola R., Berggren M. (2009) Shape and topology optimization of an acoustic horn-lens combination. Published online in *J. Comput. Appl. Math.*, doi:10.1016/j.cam.2009.08.028.
Contributions: Numerical implementation and experiments were done jointly with the first author. Writing the manuscript and developing ideas done in close cooperation with co-authors.
- III Udawalpola R., Wadbro E., Berggren M. (2010) Optimization of variable mouth acoustic horn. Submitted to *Int. J. Numer. Meth. Engng.*
Contributions: Implemented the method and performed all numerical experiments. Preparation of draft version of the manuscript. Ideas were developed in discussion with the co-authors. Completion of the manuscript was done in close cooperation with co-authors.
- IV Noreland. D., Udawalpola R., Berggren M. (2010) A Hybrid scheme for bore design optimization of a brass nstrument. Submitted to *J. Acoust. Soc. Amer.*
Contributions: Implemented and performed all numerical experiments for the Finite Element model in the hybrid scheme. Assisted in preparing the manuscript.
- V Noreland. D., Udawalpola R., Seoane P., Wadbro E., Berggren M. (2010) An efficient loudspeaker horn designed by numerical optimization: an experimental study. *Report UMINF 10.01, Umeå University, Sweden.*
Contributions: Implemented the method and performed all numerical experiments. Assisted in preparing the manuscript. Ideas were developed in close cooperation between the authors.

Contents

1	Introduction	1
2	Shape Optimization	3
2.1	Introduction	3
2.2	Shape Parameterization	4
2.3	Optimization Algorithms	4
2.3.1	Gradient-based Optimization	5
2.3.2	Alternative Methods	7
3	Acoustic Horn Optimization	9
4	Summary of Papers	11
4.1	Introduction	11
4.1.1	Model	11
4.1.2	Observations	12
4.1.3	Parameterization and Smoothing	13
4.1.4	Mesh Deformations	15
4.1.5	Optimization	16
4.2	Paper I	17
4.2.1	Model	17
4.2.2	Optimization and Selected Results	18
4.3	Paper II	21
4.3.1	Model	22
4.3.2	Optimization and Selected Results	23
4.4	Paper III	25
4.4.1	Model	26
4.4.2	Selected Results	26
4.5	Paper IV	29
4.6	Paper V	33
5	Summary in Swedish	35
6	Acknowledgment	37
	Bibliography	39

1. Introduction

The invention of the computer has resulted in a rapid increase in the use of numerical simulations in engineering design processes. At present, we are able to simulate increasingly complex systems numerically due to advances in computer hardware and scientific software. Usually the initial engineering design phase involves repeated experimental testing and construction of many prototypes. This trial and error method, which mainly relies on the designer's engineering experience, continues until a satisfactory design is found. This method may be time consuming and economically not feasible with complex systems. Thus computer simulations have been established as a powerful supportive simulation tool in engineering design.

Engineering designs have become more complicated and ambitious due to the advancement of technology. The importance of designing more efficient products is growing because of the constraints on resources. Therefore, scientist and engineers focus on finding optimal solutions for a given design problem. After simulating the system numerically, it is tempting to use numerical optimization methods to find an optimal design for given set of objectives.

In numerical design optimization, we measure the performance using an *objective function*. The objective function is calculated by observation of a *state equation* which in our case, is a set of partial differential equations (PDEs) modeling the system. During the optimization procedure, we attempt to find the extrema of this objective function by changing the design. By doing so, we find the optimal shape of the design, subject to a set of objectives and side constraints.

Numerical design optimization approaches can mainly be classified into three groups of methods, namely *sizing optimization*, *boundary shape optimization* and *topology optimization*. In sizing optimization, parameters such as the length of an element, the cross sectional area of a bar, and plate thickness are used as design variables. This is the simplest form of numerical design optimization and popular in the design of load carrying elastic structures. Boundary shape optimization uses local boundary variations to obtain the optimum design. This method typically uses body-fitted meshes, which allows an accurate representation of the boundary. Therefore, boundary shape optimization is suitable for problems that are highly sensitive to boundary smoothness, such as problems exhibiting boundary layers. The limitation of boundary

shape optimization is that it only can predict the best shape within a pre-specified topology. Topology optimization is the most general form of these three methods. The *material distribution method* for topology optimization finds the optimal design by determining the best possible distribution of material in a specified region through manipulation of coefficients in the governing equations. Thus it can predict very complex topologies. This makes topology optimization suitable for the initial design phase. The main disadvantage of this method is that it represents boundaries using a staircase approximation. Thus the method is not suitable for problems with high sensitivity to boundary smoothness. These three methods can be used in different phases of the design process. One recent example of such a design optimization process is a project at Airbus UK Ltd. [32], where design optimization was applied to such a complex problem as the internal structural design of the A380 leading edge wing. The initial design was obtained using topology optimization, and it was further optimized using size and boundary shape optimization.

2. Shape Optimization

2.1 Introduction

Shape optimization has a long history. The first documented shape optimization design problem goes back at least to the 17th century [47]. In 1638, Galileo Galilei, in his famous book *Discourses and Mathematical Demonstrations Relating to Two New Sciences (Discorsi e dimostrazioni matematiche, intorno a due nuove scienze)* [14], formulated and solved a problem of finding the optimal shape of a cantilever beam. In the 1680s Isaac Newton addressed the problem of finding the optimal shape of axisymmetric bodies of minimum drag in fluids. According to Goldstine [16] and Stein and Wiechmann [47], this problem is considered to be the first real problem of calculus of variation. Since then many scientists, like Johann and Jacob Bernnolli, Euler, Lagrange, and Weierstrass, contributed to the development of the calculus of variation [16], which became the foundation for optimal control and optimal shape design.

Modern optimal shape design field is said to have started with the work by Hadamard [19] in 1910. According to Pironneau [43], Hadamard may be the first to derive a formula for the sensitivity of a Partial Differential Equation with respect to the shape of its domain. The computer era developments were in large part initiated in the early 1970s, through the French school of applied mathematics by researchers like Cea, Glowinski, and Pironneau.

Boundary shape optimization has been widely used in structural optimization [12, 20, 23, 33] and in fluid mechanics and aerodynamic shape optimization [2, 3, 25, 34, 42]. Boundary shape optimization techniques are also used by other research disciplines such as electromagnetics [5, 11, 17, 52] and acoustics [6, 22, 29, 35].

The general shape optimization problem can be expressed as

$$\begin{aligned} \min_{\Omega \in \mathcal{Z}} J(\Omega, u), \quad \text{subject to} \\ F(\Omega, u) = 0, \\ g_i(\Omega, u) = 0, \\ h_i(\Omega, u) \leq 0. \end{aligned}$$

\mathcal{U} is a set of admissible design domains and u is the state variable. The equality constraints F is the *state equation* and the functions h_i and g_i are side constraints.

2.2 Shape Parameterization

Many different parameterization methods are used in boundary shape optimization [12, 20, 45]. Choosing a proper shape parameterization is crucial because the optimization algorithm cannot reach beyond the chosen parameterization. Therefore the optimal design achieved by the algorithm can vary with different parameterization methods.

One method of representation is to specify discrete mesh points at the boundary. This method generates a large number of design variables compared to other methods. But it can represent complex curves and shapes with high accuracy. The drawback of this method is that it may result unwanted non-smoothness in the design. To produce smooth designs, this method benefits from the use of some smoothing techniques. In our experiments we use design variables that specify the positions of discrete mesh points indirectly in order to avoid this unwanted non-smoothness. The number of design variables generated with this technique is still typically equal to the number of mesh points at the design boundary.

Another popular approach is to use polynomials and splines to represent the design boundary. The advantages of using such methods are that it requires fewer number of design variables and produce smooth boundaries. But the local controllability of the shape can be difficult. Further it is difficult to represent complex boundaries solely by polynomials and splines. The use of basis vectors or macro elements combining small elements to represent the boundary are two other popular methods. Samareh [45] discusses many shape representation techniques used in shape optimization.

2.3 Optimization Algorithms

A nonlinear optimization algorithm is an iterative procedure that starts with an initial guess and improves it in the feasible region to find the extrema of the objective function. Optimization algorithms are divided into two classes, *local search* and *global search* algorithms. Local search algorithms, also called *local optimization algorithms*, only search in the neighborhood of the current state. These algorithms cannot guarantee that the solution is globally optimal. The global search algorithms, also called *global optimization algorithms*, aim to find the global optimal. Finding the global optimum is a very difficult problem since in general we need to

the search whole feasible space to guarantee global optimality. Readers may refer to the book by Nocedal and Wright [39] for nonlinear numerical optimization algorithms.

The objective functions of shape optimization problems are usually nonlinear and have more than one local optimum. Both local and global optimization algorithms are popular in shape optimization applications. Global optimization algorithms are only feasible when using small number of design variables, whereas local optimization algorithms can be used also in the case of large number of design variables.

2.3.1 Gradient-based Optimization

We use *gradient-based* local optimization algorithms in this thesis. The simplest form of gradient-based method is the *steepest descent method*, which is easy to implement but usually not very efficient. Many standard gradient-based optimization algorithms have been applied to shape optimization. The *BFGS quasi-Newton method*, *Sequential Quadratic Programming (SQP)*, *Levenberg-Marquardt method*, and the *Method of Moving Asymptotes (MMA)* are some of the popular gradient-based algorithms used in shape optimization.

In papers I, III, IV, and V, we use `lsqnonlin` with "largescale" option, contained in Matlab's optimization toolbox, which is a trust region method based on the interior-reflective Newton algorithm [9], and in papers II and IV, we use the Method of Moving Asymptotes algorithm [48]. Usually gradient-based methods are faster and more efficient than gradient free methods provided that we can find the gradients of the objective function efficiently.

The convergence properties of the optimization algorithm typically depends on the accuracy of the supplied gradients. The calculation of gradients is typically the most time consuming part in an optimization procedure. Thus the gradient calculation of the objective function and the constraints is the most crucial step in gradient-based algorithms. Therefore we require methods to calculate gradients accurately and efficiently.

The finite difference technique is the easiest way to calculate gradients. The implementation of this method is straightforward because we only need repeated evaluations of the objective function. Therefore we can use the finite difference technique with black-box software. The drawback of this method is that it needs as many solutions to the state equation as the number of design variables. When the number of design variables and the cost of solving the state equation increase, this method becomes excessively expensive to use in shape optimization. The other disadvantage is that it may produce gradients which are not accurate enough for the optimization algorithm to converge.

2.3.1.1 The Adjoint Method

The *adjoint method* for calculating gradients is often advantageous to use in boundary shape optimization. The computational cost of calculating gradients using the adjoint method does not depend on the number of design variables, but on the number of objective functions. Therefore the adjoint method is very effective when there are large number of design variables, but relatively few objective functions and constraints. In fluid dynamics, Pironneau [42] and in aerodynamic optimizations, Jameson [24, 26, 27, 28] pioneered the use of the adjoint method. The adjoint method has been used in shape optimization problems in many occasions [4, 5, 38, 53].

There are two approaches for calculating gradients with the adjoint method, namely the *continuous adjoint method* and the *discrete adjoint method*. Giles and Pierce discuss these two approaches in the context of computational fluid dynamics [15]. The difference between the methods is in the way the gradient expressions are derived. In the continuous approach, the adjoint PDE is derived from the state PDE in continuous form, that is, before discretization. Then the adjoint PDE is discretized to calculate adjoint variables. But in discrete method, the adjoint equation is derived directly from discretized state PDE. These two approaches typically give completely different final expressions. Nadarajah and Jameson [36, 37] have compared the complexity and the accuracy of both methods for aerodynamic shape optimization. A discussion on the merits of the continuous and discrete approaches can also be found in chapter 2.9 of the book by Gunzburger [18]. The implementation of the adjoint method involves a large coding effort and usually requires the access to the source code of the software.

We use the discrete adjoint method in papers I, II, IV, and V. The discrete adjoint method can calculate exact (up to machine precision) gradients of discrete objective functions if we can solve the discretized state and adjoint equations exactly. The finite element method (FEM), which is used in papers I, II, IV and V to discretize the PDEs, solves the discretized equations exactly. Therefore the discrete adjoint method was preferred with the FEM. In paper III, where we use the boundary element method (BEM) to discretize the system, the continuous adjoint method is used to calculate gradients. We use an adaptive quadrature to evaluate the integrals in the BEM. Differentiation of the discretized integral equation together with adaptive quadrature was regarded too complicated to handle. Therefore we opt to use the continuous adjoint method with the boundary element method discretization.

2.3.1.2 Automatic Differentiation

The implementation of the adjoint method for gradient calculations involves a tedious effort of deriving expressions and a large coding effort. The finite difference method is simple and easy to implement but suffers from

both round off errors and truncation errors. The technique of *automatic differentiation* appeared as an easy alternative to minimize human effort and truncation errors.

Automatic differentiation can be implemented in two different ways, using *source code transformation* or *operator overloading*. In the source code transformation technique, the source code is replaced by another which contains statements for calculating derivatives. The operator overloading approach can be carried out in languages such as C++ which has support for it. In this approach, the arithmetic operators are redefined to perform simultaneous functional and derivative calculations.

There are two methods of automatic differentiation, the *forward mode* and the *reverse mode*. A detailed description about these methods can be found in chapter 8 of the book by Nocedal and Wright [39]. The computational complexity of automatic differentiation forward mode is similar to the finite difference technique. Therefore it is not efficient for problems with many design variables. The reverse mode of automatic differentiation, which corresponds to the adjoint method, has high memory requirements for the storage of intermediate variables.

2.3.2 Alternative Methods

The tediousness involved in calculating gradients efficiently may be one of the reasons for the popularity of gradient-free optimization methods in engineering design. Another reason is that in commercial software packages, we do not have access to the source code, which is usually required for efficient calculation of gradients. Further, the gradient-based methods can not be used with problems in which design variables are discrete.

Genetic Algorithm, *Simulated Annealing* and *Hill Climbing* are examples for gradient-free methods that have been used for shape optimization [8, 52]. Genetic algorithm and simulated annealing are global search algorithms, whereas the hill climbing algorithm is a local search method. Usually, these methods require a large number of the objective function evaluations. When the cost of evaluating the objective function is high, these algorithms become costly.

The number of function evaluations during the optimization process is a critical factor. Surrogate-model based optimization is a popular technique in design optimization to reduce the number of function evaluations. These surrogate models build an approximate model for the objective function and then use local or global search methods to find the optimum [44]. The surrogate model is computationally inexpensive to evaluate and is therefore used by the optimization algorithm in order to reduce the number of expensive function evaluations.

3. Acoustic Horn Optimization

A horn is an interfacial device, situated between a source, such as a waveguide or a transducer, and surrounding space. Horns are usually used to control the transmission properties from the source and the spatial power distribution in the far field. In acoustics, horn-like devices are used in brass instruments and in loudspeaker systems designed for large halls or outdoor use.

The horn is one of the first musical instruments or signaling devices used by humans. The curiosity and creativity of humans have resulted in many different kinds of horns either for use as a musical instrument or as a sound-enhancing device. One difference between loudspeaker horns and musical instrument horns is that musical horns need to initiate standing waves inside the instrument for the production of sound, whereas loudspeaker horns simply are used to transmit sound energy efficiently. A unique feature of musical horns is that they are tapered to obtain a harmonic spacing of the standing waves.

Human ears are very sensitive to subtle differences in sound. Therefore the numerical models for acoustics, specially for musical instruments, should be able to predict these differences. There are many numerical methods for analyzing impedance and radiation properties of acoustic horns. These methods vary from one dimensional transmission line models to two or three dimensional finite element and boundary element methods. But surprisingly, in the literature, there are very few attempt to design acoustics horns with desired set of properties using numerical optimization.

In the 1970s Alfredson [1] presented a model to predict radiation patterns and claimed that the method could be extended to predict the shape of the horn flare required to produce a particular radiation directivity pattern. Henwood [22] used the boundary element method to design an acoustic tweeter where he used single spline to represent the horn profile.

Bångtsson et al. [4] used boundary shape optimization to improve the efficiency of horns with planar symmetry. They used the finite element method to analyze the horn. The BFGS quasi-Newton method was used for optimization and the gradients were supplied using the adjoint method. They managed to obtain transmission-efficient smooth horns shapes within a given frequency band.

Wadbro and Berggren [50, 51] used topology optimization to improve efficiency and to control directivity properties of a horn with planar symmetry. Very interesting horn shapes were obtained. They used the Method of Moving Asymptotes for optimization where gradients were supplied using the adjoint method. Specifically they managed to optimize a horn for a low frequency band to obtain a horn shape similar to a *folded horn*.

In Paper I, we optimize horns with planar and cylindrical symmetries. Boundary shape optimization is used to obtain transmission-efficient horns for a pre-specified frequency band. Further we optimize horns with respect to directivity to obtain uniform far-field patterns. The Matlab `lsqnonlin` large scale method is used and gradients are supplied with the adjoint method.

Morgans et al. [35] optimized an axisymmetric horn to obtain constant *beamwidth* for wide frequency band using Efficient Global Optimization (EGO), which is a surrogate method. The boundary element method was used to analyze the horn where the horn shape was represented using a spline with two control points. They obtained a horn with mean beamwidth of 47.1° degrees throughout the frequency band of interest.

In Paper II, we optimize a horn-lens combination to obtain transmission-efficient horn with a beamwidth higher than 100° for the frequency band 250 Hz – 1000 Hz. Simultaneous shape and topology optimization is used for designing the horn-lens combination. The MMA algorithm solves the optimization problem using gradients supplied by the adjoint method.

In the 1970s Smith and Daniell [46] developed a method to correct the intonation in wind instruments by perturbing the bore diameter. Later Kausel [29] used the Rosenbrock algorithm and five different genetic algorithms to reconstruct the bore of a brasswind instrument. The instrument was represented by cylindrical or conical segments. Noreland [40] used the Levenberg-Marquardt gradient-based optimization method to design brasswind instruments. The instrument is approximated by a series of conical waveguide elements. Recently, Braden et al. [7] used the Rosenbrock method to construct the bore of a trombone. They approximated the instrument with a series of Bessel horns.

The most of the brasswind optimization work mentioned above use the *Transmission Line* (TL) model to analyze the instrument. The problem with this model is that it may not be accurate enough in the rapidly varying part. In paper IV, we use a hybrid method where a one dimensional TL model is used to analyze the slowly flaring part and the two dimensional FEM in the rapidly flaring part near the mouth. Gradient-based algorithms are used for optimization. The gradients are supplied both analytically and using the adjoint method.

4. Summary of Papers

4.1 Introduction

In this thesis, we optimize acoustic horns with both planar and cylindrical symmetries. We optimize loudspeaker horns to obtain high transmission efficiency and preferred directivity patterns. Brass wind instruments are optimized with respect to intonation properties. This chapter contains a general description of the optimization model and a short summary of each included paper.

4.1.1 Model

We assume that the sound propagation in exterior domain Ω , illustrated in Figure 4.1, is governed by the linear wave equation

$$\frac{\partial^2 P}{\partial t^2} - c^2 \Delta P = 0, \quad (4.1)$$

where c is the speed of sound, P is the acoustic pressure and Δ is the Laplacian operator. Using the ansatz $P(x, t) = \Re\{p(x)e^{i\omega t}\}$, we seek time harmonic solutions of the wave equation for the complex amplitude function p at frequency ω . Thus we obtain that p satisfies the *Helmholtz equation*

$$\Delta p + k^2 p = 0 \quad \text{on } \Omega, \quad (4.2a)$$

$$ikp + \frac{\partial p}{\partial n} = 2ikA \quad \text{on } \Gamma_{\text{in}}, \quad (4.2b)$$

$$\frac{\partial p}{\partial n} = 0 \quad \text{on } \Gamma \setminus \Gamma_{\text{in}}, \quad (4.2c)$$

$$\lim_{|x| \rightarrow \infty} |x|^{(d-1)/2} \left(\frac{\partial p}{\partial |x|} + ikp \right) = 0 \quad \text{uniformly in all directions,} \quad (4.2d)$$

where $k = \omega/c$ is the wave number and $d = 2$ or 3 is the number of dimensions. Here n is the normal to the boundary of the domain. Boundary condition (4.2b) specifies a *right going wave* of amplitude A at boundary Γ_{in} and absorbs all *left going waves*. Sound hard boundaries are described with boundary condition (4.2c), and (4.2d) is the Sommerfeld radiation condition.

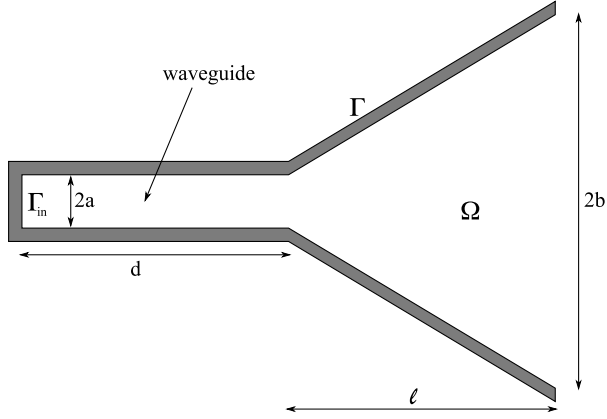


Figure 4.1: The horn model and domain of wave propagation.

4.1.2 Observations

Wave propagation for a wave with wave number k , in the *waveguide* illustrated in Figure 4.1, consists of right-going (input wave) wave with amplitude A and left-going (reflected wave) wave with amplitude B ; both A and B are in general complex numbers. To measure efficiency we observe the *reflection coefficient*. The reflection coefficient for a wave with wave number k can be defined as

$$R_k = \frac{B}{A}. \quad (4.3)$$

We plot absolute value of the reflection coefficient against frequency in plots of the *reflection spectrum*.

To calculate *far-field directivity patterns*, we observe the magnitude of pressure far away from the sound sources at a given angle θ . (Note that when considering planar and cylindrical symmetry in horns, the far-field directivity patterns also have corresponding symmetry.) From classical methods of scattering theory [10], we can derive an expression for far-field directivity patterns. We recall the asymptotic behavior of the solution to the Helmholtz equation p for planar ($d = 2$) or axisymmetric ($d = 3$) symmetry. Let \hat{x} be a unit vector in the direction of angle θ and ρ a positive scalar. The asymptotic behavior of p as $\rho \rightarrow \infty$ for dimension d is

$$p(\rho\hat{x}) = \frac{e^{-ik\rho}}{\rho^{(d-1)/2}} \left\{ p_\infty(\theta) + O\left(\frac{1}{\rho}\right) \right\}, \quad (4.4)$$

and the far-field pattern for wave with wave number k is given by

$$p_\infty(\theta, k) = c_d \int_{\bar{\Gamma}} e^{ik\hat{x}\cdot x} \left[ikp\hat{x}\cdot n - \frac{\partial p}{\partial n} \right] d\Gamma, \quad (4.5)$$

where c_d depends on the space dimensions:

$$c_2 = \frac{1-i}{4\sqrt{\pi}k} \quad \text{and} \quad c_3 = \frac{1}{4\pi}. \quad (4.6)$$

Here $\tilde{\Gamma}$ is a closed surface surrounding all sound sources. Wadbro [49] has given a detailed derivation of above expressions.

Polar plots of $|p_\infty(\theta, k)|^2$ in decibel (dB), that is, plots of $20\log_{10}|p_\infty(\theta, k)|$, are used to illustrate the far-field directivity patterns. The *beamwidth* of a device at wave number k is defined as the angle between the -6 dB points closest to the horn axis of the relative directional intensity

$$d(\theta) = 20\log_{10}\left(\frac{|p_\infty(\theta, k)|}{\max_\theta |p_\infty(\theta, k)|}\right).$$

For brasswind instruments the *input impedance spectrum* is an important characteristics. Assuming one-dimensional propagation of a wave with angular frequency ω , the input impedance, $Z_{\text{in}}(\omega)$, can be defined as

$$Z_{\text{in}}(\omega) = \frac{p_{\text{in}}(\omega)}{U_{\text{in}}(\omega)}. \quad (4.7)$$

where $U_{\text{in}}(\omega)$ is the acoustic volume flow velocity and $p_{\text{in}}(\omega)$ the acoustic pressure. The relation between acoustic impedance and reflection coefficient is

$$R = \frac{Z_{\text{in}} - \rho c/S}{Z_{\text{in}} + \rho c/S}, \quad Z_{\text{in}} = \frac{1+R}{1-R}\rho c/S, \quad (4.8)$$

where c is the speed of sound, ρ is the density, and S the input cross sectional area [30].

4.1.3 Parameterization and Smoothing

We use the normal distance from the *reference shapes* Γ_d^{ref} , depicted in Figures 4.2 and 4.3 to the node points in the design boundary to represent the shape. That is, we represent each point x_d in the design boundary Γ_d as

$$x_d = x_{\text{ref}} + \beta(x_{\text{ref}}) n_{\text{ref}}, \quad (4.9)$$

where β is the normal displacement function from the reference shape and n_{ref} is the normal to the reference shape. We use two reference shapes during our experiments. As the first reference shape $\Gamma_d^{\text{ref}_1}$, we use the conical horn surface as illustrated in Figure 4.2. We use a line parallel to the horn axis as the second reference shape $\Gamma_d^{\text{ref}_2}$, as illustrated in Figure 4.3.

The direct use of β as our design variable will result in wiggly shapes in the optimized horns, as reported by Bångtsson et al. [4]. Therefore we in-

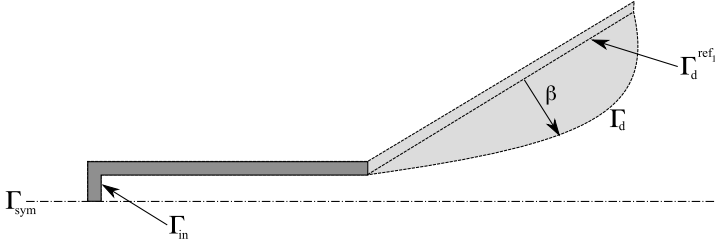


Figure 4.2: Parameterization perpendicular to a conical horn reference shape.

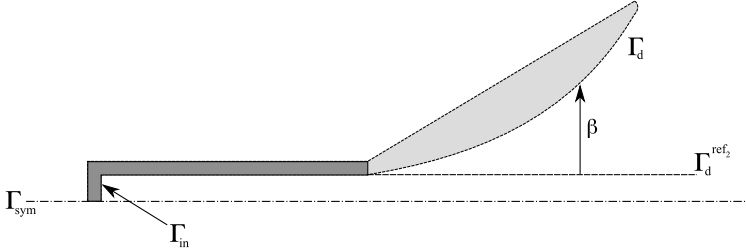


Figure 4.3: Parameterization perpendicular to the symmetry axis of the horn.

roduce a new design variable η and specify β indirectly as a solution to a boundary value or initial value problem. We use three different parameterization techniques.

In parameterization *type 1*, we use η as our design variable, and β , which is the perpendicular distance from $\Gamma_d^{\text{ref}1}$, is defined as the solution to the boundary value problem

$$\begin{aligned} \beta'' &= \eta && \text{in } \Gamma_d^{\text{ref}1}, \\ \beta &= 0 && \text{on } \partial\Gamma_d^{\text{ref}1}. \end{aligned} \quad (4.10)$$

In parameterization *type 2*, we use η as our design variable, and β , which is the perpendicular distance from $\Gamma_d^{\text{ref}2}$, is defined as the solution to the initial value problem

$$\begin{aligned} \beta'' &= \eta && \text{in } \Gamma_d^{\text{ref}2}, \\ \beta'(0) &= 0, \\ \beta(0) &= 0. \end{aligned} \quad (4.11)$$

Parameterization *type 3* uses η as the design variable, and β , which is similar to parameterization type 2, is defined as the solution to the initial value

problem

$$\begin{aligned} \beta' &= \eta && \text{in } \Gamma_d^{\text{ref}_2}, \\ \beta(0) &= 0. \end{aligned} \quad (4.12)$$

Parameterization type 1 keeps the ends of design boundary fixed. The end width of the design boundary is allowed to vary in parameterization of type 2 and 3. If required, we can keep the end width fixed during optimization by imposing an equality constraint for parameterizations of type 2 and 3.

4.1.4 Mesh Deformations

The design boundary is modified during the optimization procedure. When using full domain discretization methods as the finite element method for shape optimization, we need to adjust the mesh nodes inside the computational domain to preserve the mesh quality or perform a complete or partial remeshing. A remeshing could introduce "noise" in the objective function by adding and deleting elements in the mesh. This could hurt the convergence of the optimization algorithm. Therefore we chose instead to deform the initial mesh to conform to the modified design boundary.

During the optimization procedure, we modify every node point according to the movement of the design boundary to retain the validity and quality of the mesh. It is difficult to handle large deformation of design boundary, without creating invalid meshes or meshes of bad quality. In order to avoid too large deformations, we choose an initial design Γ_d^0 in the form of an exponential shape, associated with an orthogonal displacement β_0 of the reference design Γ_d^{ref} , that should be closer to the optimal design than Γ_d^{ref} . We triangulate the domain associated with Γ_d^0 to obtain the initial mesh from which the optimization is started.

Define

$$\mathbf{X}^0 = (x_1^0, \dots, x_N^0)^T,$$

where x_i^0 is the coordinate of mesh vertex i in the initial mesh and N is the number of vertices in the mesh. The coordinates of the vertices at the n th design cycle can be represented by a vector

$$\mathbf{X}^n = (x_1^n, \dots, x_N^n)^T, \quad (4.13)$$

where n refers to design cycle n . The optimization algorithm returns values of design variable η at the n th design cycle. The corresponding value of β is calculated by solving equations (4.10), (4.11) or (4.12) according to the

chosen parameterization. Then we numerically solve the Poisson problem

$$\Delta \mathbf{u} = 0 \quad \text{in } \Omega, \quad (4.14a)$$

$$u = g(\boldsymbol{\beta}) n_{\text{ref}} \quad \text{on } \Gamma_d^0, \quad (4.14b)$$

$$u = 0 \quad \text{on } \Gamma \setminus \Gamma_d^0, \quad (4.14c)$$

for u using the finite-element method. Here $g(\boldsymbol{\beta})$ is a piecewise linear scalar function that attains the values of $(\boldsymbol{\beta} - \boldsymbol{\beta}_0)$ at node points of Γ_d^0 . The values of u at the node points are arranged in a vector \mathbf{U} which yields a vector of mesh displacements associated with the current $\boldsymbol{\eta}$. Then we update the mesh coordinates for $(n + 1)$ th design cycle using

$$\mathbf{X}^{n+1} = \mathbf{X}^0 + \mathbf{U}. \quad (4.15)$$

Instead of solving equation (4.14) at each design cycle, we choose to pre-compute numerical solutions for unit changes of each component of the design variable $\boldsymbol{\eta}$, and store the solution as columns of a matrix \mathbf{A} . Then we can express the relationship between changes $\delta\boldsymbol{\eta}$ of the design variables and displacements $\delta\mathbf{X}$ of the mesh nodes by a linear relation

$$\delta\mathbf{X} = \mathbf{A} \delta\boldsymbol{\eta}, \quad (4.16)$$

Using matrix A to update the mesh vertex coordinates is computationally efficient in this two-dimensional settings. This strategy would not be competitive in three space dimensions due to excessive storage requirements.

4.1.5 Optimization

We optimize to obtain preferred reflection spectrum and far-field directivity patterns by changing the horn flare. The objective function is formulated as non-linear least-squares problem. For example we can represent the objective function to minimize reflection coefficient as

$$J(\boldsymbol{\eta}) = \sum_{k \in F_r} |R_k|^2, \quad (4.17)$$

where $\boldsymbol{\eta}$ is the design variable and F_r is an index set for which we need the reflections to be minimized. This problem is conceptually a non-linear least-squares problem.

A typical cure for irregular solutions is to add a *Tikhonov regularization* term to the objective function. Now the objective function can be represented as

$$J^e(\boldsymbol{\eta}) = \frac{\epsilon}{2} \int_{\Gamma_d^{\text{ref}}} \boldsymbol{\eta}^2 d\Gamma + \sum_{k \in F_r} |R_k|^2, \quad (4.18)$$

The absorbing boundary conditions together with equation (4.2) yield the state equation

$$c^2 \nabla \cdot (r \nabla p) + \omega^2 r p = 0 \quad \text{in } \Omega, \quad (4.20a)$$

$$\left(i\omega + \frac{c}{\kappa R_\Omega} \right) p + c \frac{\partial p}{\partial n} = 0 \quad \text{on } \Gamma_{\text{out}}, \quad (4.20b)$$

$$i\omega p + c \frac{\partial p}{\partial n} = 2i\omega A \quad \text{on } \Gamma_{\text{in}}, \quad (4.20c)$$

$$\frac{\partial p}{\partial n} = 0 \quad \text{on } \Gamma_n \cup \Gamma_{\text{sym}}, \quad (4.20d)$$

where $\kappa = 2$ and $r = 1$ for planar symmetry. For cylindrical symmetry $\kappa = 1$ and r is the distance to the symmetric axis.

4.2.2 Optimization and Selected Results

We optimize the horn presented in Figure 4.4 by changing the design boundary Γ_d normal to reference conical shape $\Gamma_d^{\text{ref}1}$. We use objective function (4.18) together with parameterization type 1. The convexity constraint $\eta \geq 0$ is used in the optimization procedure to obtain convex designs when required.

Figure 4.5 shows the shape and reflection spectrum of the horn with planar symmetry optimized for transmission efficiency in the frequency band 350 Hz–1150 Hz without convexity constraints. Figure 4.6 shows the shape and the reflection spectrum when optimized with convexity constraints. The horn optimized without convexity constraint shows almost perfect transmission properties throughout the frequency band but its irregular shape may not be suitable for manufacturing. When we applied the convexity constraint on the geometry, the reflections within the optimized frequency band increase slightly. On the other hand, the smoother shape has improved the transmission efficiency at the higher frequencies outside the optimized frequency band. The same experiment was repeated but with cylindrical symmetry. The resulting shape and the spectrum are shown in Figure 4.7 for the horn optimized with convexity constraints. It should be noted that, by comparing figures 4.6 and 4.7, it is more difficult to control reflections in horns with cylindrical symmetry than with planar symmetry.

The other objective of the paper is to control far-field directivity patterns by changing the horn flare. In this experiment we try to match the *far-field intensity*, the square of the absolute values of far-field directivity, in the direction of different angles at different frequencies. To achieve that, we use

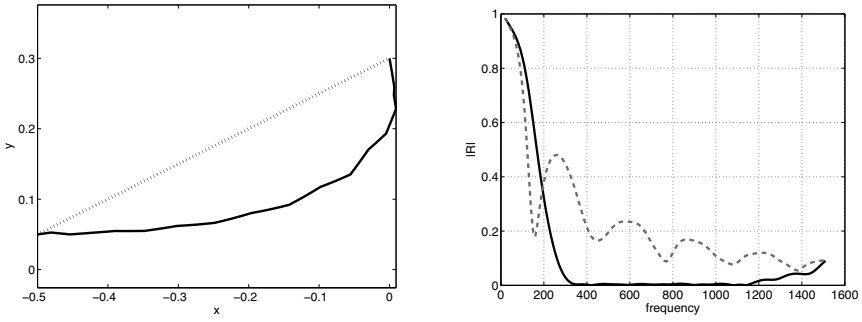


Figure 4.5: The shapes of the horns (left), reflection spectra of the horns (right) in planar symmetry optimized with no geometry constraints for a frequency band from 350 Hz to 1150 Hz at 31 frequencies (solid) and for the reference shape (dashed).

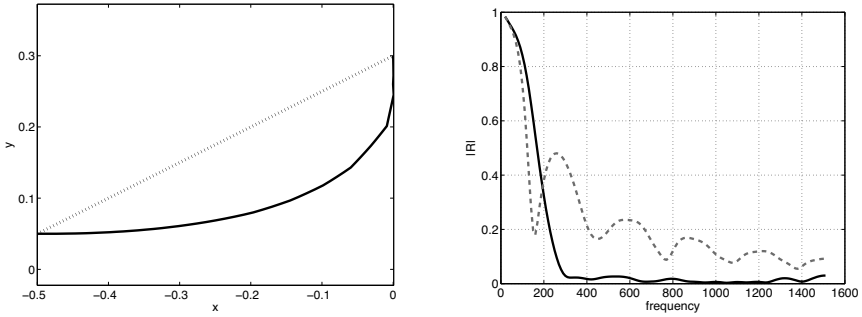


Figure 4.6: The shapes of the horns (left), reflection spectra of the horns (right) in planar symmetry optimized with convexity constraints for a frequency band from 350 Hz to 1150 Hz at 31 frequencies (solid) and for the reference shape (dashed).

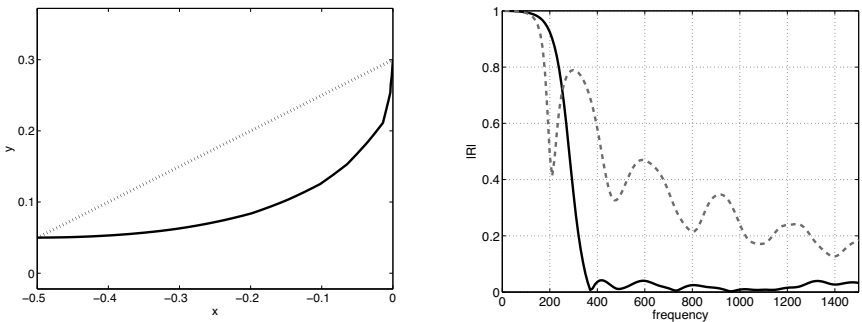


Figure 4.7: The shapes of the horns (left), reflection spectra of the horns (right) in cylindrical symmetry optimized with convexity constraints for a frequency band from 350 Hz to 1150 Hz at 31 frequencies (solid) and for the reference shape (dashed).

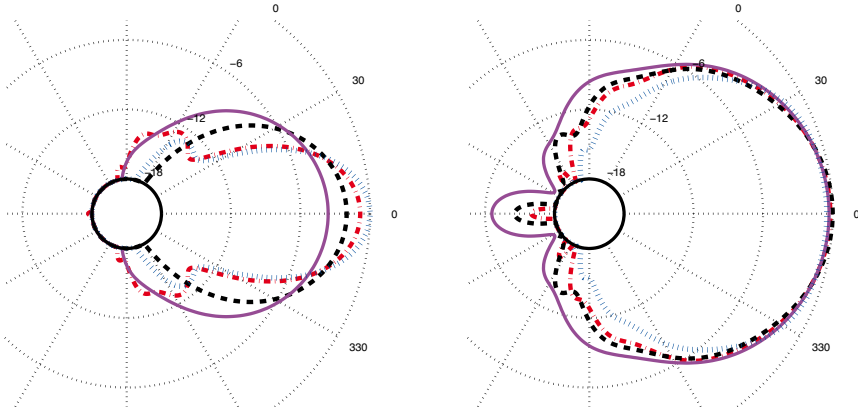


Figure 4.8: The far-field patterns at frequencies 400 Hz (solid), 600 Hz (dashed), 800 Hz (dotted-dashed), and 1000 Hz (dotted) for the horn in planar symmetry, for reference shape (left) and for optimized for far-field pattern in the directions of 0, 25, and 30 degrees (right).

the objective function

$$\begin{aligned}
 J^\epsilon(\eta) = & \frac{\epsilon}{2} \int_{\Gamma^{\text{ref}}} \eta^2 d\Gamma + \sigma_r |R_{k_r}|^2 \\
 & + \sigma_f \sum_{k \in F_f} \sum_{\theta_l} \left| |p_\infty(\theta_l, k)|^2 - |p_\infty(\theta_l, k_0)|^2 \right|^2,
 \end{aligned} \tag{4.21}$$

where F_f is the set of frequencies and θ_l are the angles at which we want to control the far-field directivity. Here k_0 is a reference frequency. Note that while attempting to obtain an even directivity patterns, we need to prevent the trivial local minimum that occurs when the intensity is zero, due to 100 percent reflection for all frequencies. Thus, we also include a term to minimize the reflections at a frequency k_r .

Figure 4.8 shows the directivity patterns of the reference horn and the horn optimized for even directivity patterns at 400, 600, 800, and 1000 Hz for angles 0° , 25° and 30° , and with minimized reflections at 400 Hz. The corresponding shape and the reflection spectrum is shown in Figure 4.9. We managed to obtain more uniform far-field directivity patterns at the angles of interest. But we have to pay the price in transmission efficiency. It should be noted that the transmission efficiency in the optimized horn is worse than the reference horn except close to 400 Hz. An analogous experiment was done for the horns with cylindrical symmetry.

Our results demonstrate that the transmission efficiency and the far-field directivity properties of acoustic horns are very sensitive to the shape of the horn flare. The results also show that we can design horns with almost perfect transmission properties within a significantly wide

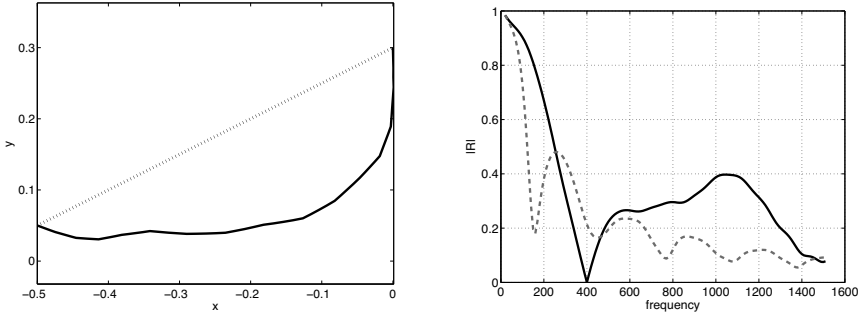


Figure 4.9: The shapes of the horns (left), reflection spectra of the horns (right) in planar symmetry for reference shape (dashed) and for optimized for far-field pattern in the directions of 0, 25, and 30 degrees (solid).

frequency band. The improvement in transmission efficiency, compared to the reference shape, is larger for the horn with cylindrical symmetry, even though the reflections in the optimized cylindrical horn is slightly higher than the optimized planar horn. The improvement in transmission efficiency is particularly pronounced at lower frequencies, since the efficiency for the reference horn was low in this region.

Directly optimizing with respect to directivity is more delicate. To obtain meaningful results, we found it necessary to include also a term involving the reflection in the objective function. We have demonstrated that it is possible to obtain more uniform far-field directivity patterns with respect to frequency. However, the penalty on the efficiency is high. To obtain more detailed control over the far-field directivity without too much penalty on efficiency, it may be necessary to include additional acoustical components, such as an acoustic lens.

4.3 Paper II

In paper I we found that it may be difficult to control both the transmission efficiency and the far-field directivity at the same time only by changing the horn flare. Therefore in paper II we optimize a horn–lens combination, which is inspired by the classical horn–lens combinations conceived by Kock and Harvey [31] in the 1940s, to control both transmission efficiency and far-field directivity patterns. Here, we use shape and topology optimization simultaneously to design a transmission efficient horn–lens combination with even directivity for a wide range of frequencies.

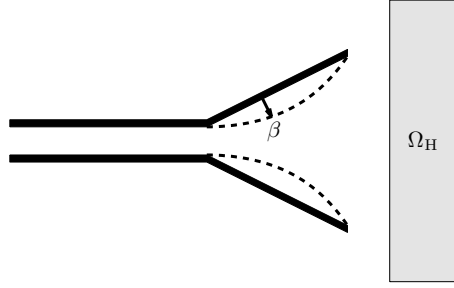


Figure 4.10: The walls of the horn are displaced and material is placed in the region Ω_H to improve the radiation properties.

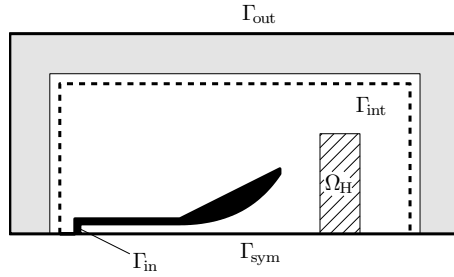


Figure 4.11: The computational domain Ω .

4.3.1 Model

The setup used as a basis for optimization, illustrated in Figure 4.10. The geometry is assumed to be infinite in the direction normal to the plane. The device consists of a waveguide with a conical termination (the horn) and a lens located in front of the horn.

We solve wave propagation problem (4.2) numerically using the finite element method. The unbounded domain is truncated to a rectangular domain using a perfectly matched layer (PML), marked gray in Figure 4.11, to handle the outgoing wave property. Following Heikkola et al. [21], we define

$$\gamma_k = 1 - i\sigma_0 \frac{\sigma_k}{\omega}, \quad k = 1, 2, \quad \gamma = \gamma_1 \gamma_2, \quad D = \begin{pmatrix} \gamma_2 / \gamma_1 & 0 \\ 0 & \gamma_1 / \gamma_2 \end{pmatrix},$$

where σ_0 is a non-negative constant,

$$\sigma_1 = \max\left(0, \max\left(x_1 - \bar{x}_1 + \delta, \underline{x}_1 + \delta - x_1\right)\right), \quad \sigma_2 = \max\left(0, x_2 - \bar{x}_2 + \delta\right),$$

and where x_1 and \bar{x}_1 are the coordinates for the left and right edge of the computational domain Ω , depicted in Figure 4.11, respectively. Similarly, \bar{x}_2 corresponds to upper edge, and δ is the width of the PML layer. We modify

equation (4.2) to include the PML as follows:

$$\nabla \cdot (D\nabla p) + k^2 \gamma p = 0 \text{ in } \Omega. \quad (4.22)$$

Petropoulos [41] reports that the boundary condition terminating the PML does not have a significant effect on accuracy when the loss profile is linear or quadratic. In our experiments, we use boundary condition (4.2c) at the outer boundary Γ_{out} .

4.3.2 Optimization and Selected Results

We optimize the horn–lens combination presented in Figure 4.10, allowing the horn flare to deflect normal to the funnel-shaped reference flare and allowing sound hard material to fill an arbitrary region within Ω_H . The parameterization type 1 is used to represent the horn flare. The function α is defined in Ω_H , such that for any point x , $\alpha(x) = 0$ if x is a solid material point and $\alpha(x) = 1$ if x is air. We use objective function

$$J(\eta, \alpha) = \sum_{\omega_m} \left(|R_k|^2 + \sigma_b \sum_{\vartheta_b} \left| |p_\infty(\vartheta_b, k)|^2 \right|^2 + \sigma_f \sum_{\theta_l} \left| |p_\infty(\theta_l, k)|^2 - |p_\infty(\theta_0, k)|^2 \right|^2 \right), \quad (4.23)$$

to minimize reflections and control far-field patterns, in which ω_m is the set of frequencies for which we minimize reflections and control far-field directivity. We minimize far-field directivity patterns at angles ϑ_b . Usually these angles are selected to reduce *back scattering*. We also minimize the difference of directivity patterns between angles θ_l and θ_0 which is the reference angle.

The next step is to introduce a penalty term such as

$$J_p = \int_{\Omega_H} (\alpha - \varepsilon)(1 - \alpha) \, d\Omega,$$

in the objective function to promote values close to ε or 1 for α . Unfortunately, the addition of such a term aggravates the ill-posedness of the optimization problem. An issue related to the ill-posedness problem is the lack of control over the size of the structural parts. We therefore introduce a new design variable $\tilde{\alpha}$ and define α indirectly through the convolution $\alpha = K_\tau * \tilde{\alpha}$, where K_τ is an integral operator kernel with support in a neighborhood of radius τ that provides a local averaging of the design variable.

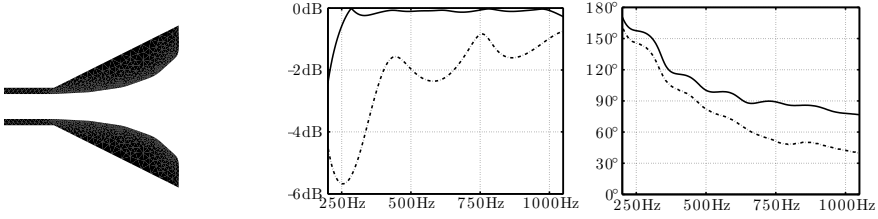


Figure 4.12: Horn without lens optimized for high transmission efficiency and even directivity using only modifications of the horn flare (left), the transmission loss in dB (middle), and the beamwidth (right) as functions of frequency. The dash-dotted lines in the diagrams illustrate efficiency and directivity properties for our funnel shaped reference horn.

We thus state our general optimization problem as

$$\min_{\tilde{\alpha}, \eta} \left[\sigma_{\eta} \int_{\Gamma_{\text{ref}}} \eta^2 d\eta + \sigma_{\alpha} \int_{\Omega_H} (K_{\tau} * \tilde{\alpha} - \varepsilon)(1 - K_{\tau} * \tilde{\alpha}) d\Omega + J(\eta, K_{\tau} * \tilde{\alpha}) \right], \quad (4.24)$$

where the first term is a Tichonov regularization term for the horn flare and the second term provides penalty and filtering. The constants σ_{η} and σ_{α} are used specify the amount of regularization and penalty, respectively. The Method of Moving Asymptotes is used in the optimization.

In our experiments, we aim for a high efficiency and a 100° beamwidth in the two-octave-wide frequency range 250–1000 Hz. We therefore optimize the device for even directivity at the angles $0^{\circ}, \pm 10^{\circ}, \dots, \pm 50^{\circ}$ with respect to the horn axis for frequencies exponentially spaced with 12 frequencies per octave. The angles 90° and 180° are used to minimize the back scattering. That is, we set the frequencies and angles in objective function (4.23) as follows: $\omega_m = 250 \cdot 2^{m/12}$, $m = 0, 1, \dots, 24$, $\theta_l = l \cdot 10^{\circ}$, $l = 0, 1, \dots, 5$, $\vartheta_0 = 180^{\circ}$, and $\vartheta_1 = 90^{\circ}$.

Figure 4.12 shows the reflection spectra and beamwidth comparisons between the reference horn and the horn optimized with only changing the horn flare. From the figure we can see that there is a decreasing trend in beamwidth for both shapes. The beamwidth at 1000 Hz is under 80° for the optimized horn and under 40° for the reference horn. Figure 4.13 shows the reflection spectra and beamwidth of the optimized horn–lens combination. It is clear that we manage to keep the beamwidth above 105° throughout the frequency band.

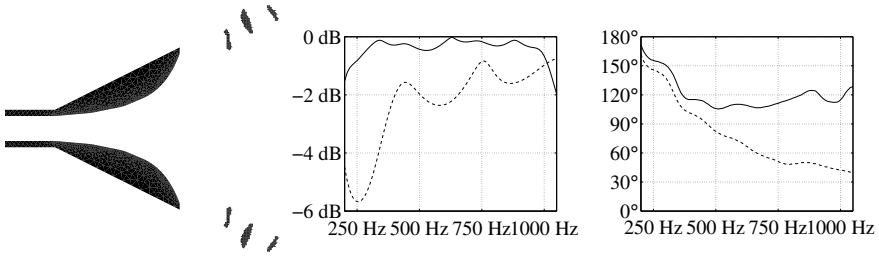


Figure 4.13: Horn-lens combination optimized for high transmission efficiency and even directivity (left), the transmission loss in dB (middle), and the beamwidth (right) as functions of frequency. The dash-dotted lines in the diagrams illustrate efficiency and directivity properties for our funnel shaped reference horn.

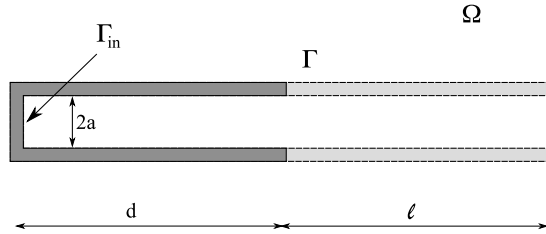


Figure 4.14: Profile of initial waveguide and domain of wave propagation Ω . Γ is the domain boundary and boundary Γ_{in} specifies right going wave with magnitude A .

4.4 Paper III

The objective of this paper is to construct transmission efficient horn-like devices evolving from a waveguide. The mouth diameter of the device, that is, the diameter of the opening towards free space, will *not* be specified a priori; the mouth diameter will be a result of the optimization. We let the light-colored part of the waveguide illustrated in Figure 4.14 evolve to form a transmission efficient device for pre-specified frequency band.

Parameterization of type 2 and type 3 are used here. These methods allows us to have a variable diameter. Allowing variable mouth width cause substantial deformation of the design boundaries. Full domain discretization methods such as the finite element method may be inefficient for optimization problems with large boundary deformations. This made the boundary element method into an attractive option, because it only needs discretization of the boundary of the domain.

4.4.1 Model

The boundary integral formulation

$$\begin{aligned} \frac{1}{2}p(x) + ik \int_{\Gamma_{\text{in}}} p(y) d\Gamma(y) + \int_{\Gamma} p(y) \frac{\partial G_x(y)}{\partial n_y} d\Gamma(y) \\ = 2ikA \int_{\Gamma_{\text{in}}} G_x(y) d\Gamma(y), \end{aligned} \quad (4.25)$$

where

$$G_x(y) = \frac{e^{-ik|x-y|}}{4\pi|x-y|}$$

is the fundamental solution of Helmholtz equation in three dimensions, of governing equation (4.2) holds for each $x \in \Gamma$ such that Γ is smooth at x .

The Boundary Element Method (BEM) numerically solves integral equation (4.25). The horn surface is discretized with N conical axisymmetric elements. We use the C^0 collocation method, that is, we assume that the acoustic pressure is constant throughout each element.

For the optimization of the flare shape, we solve the following least squares problem

$$\begin{aligned} \min_{\boldsymbol{\eta}} \quad & \sum_{f \in F} |R_f|^2 + \varepsilon \langle \boldsymbol{\eta}, \boldsymbol{\eta} \rangle \\ \text{s.t.} \quad & \boldsymbol{\eta} \geq 0 \end{aligned}$$

where F is a set of frequencies for which we want to minimize the reflections back to the waveguide. The last term is a Tichonov regularization for the flare shape; in the numerical experiments presented in this section we solve the problem with parameter $\varepsilon = 10^{-8}$. We use Matlab's function `lsqnonlin` with default termination conditions to solve the above optimization problem. The continuous adjoint approach is used to calculate gradients of the objective function.

4.4.2 Selected Results

We start by optimizing a horn using parameterization type 1 for frequency band 523–880 Hz, minimizing the reflection at the 10 frequencies $440 \cdot 2^{m/12}$ Hz, where $m = 3, 4, \dots, 12$, that is, all semitones from C5 to A5. Figure 4.15 shows snapshots from the optimization of the interfacial device. The upper row shows the initial shape (left) and the shape after one (middle) and five (right) iterations. This row illustrate that in the beginning of the optimization process the most important single feature that improves the performance is the opening of the device *mouth*. The middle row shows (from left to right) the design after 10, 20, and 30 iterations, where the optimization routine continues opening the mouth of the device. However, we can also

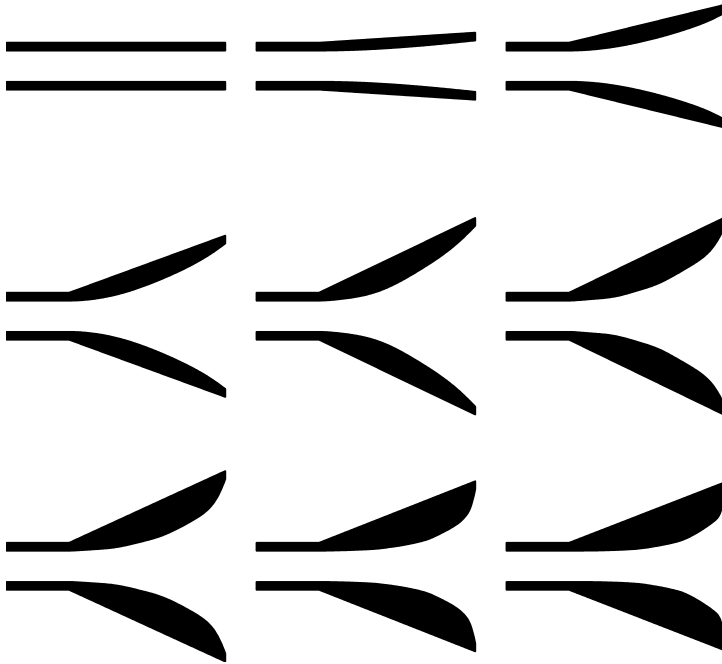


Figure 4.15: Optimization of convex horn for frequency band 523–880 Hz. The shapes show the evolution of the interfacial device throughout the optimization process from initial tube (upper left) to final optimized horn (bottom right). The shapes show the device after (starting with the upper row from left to right) 0, 1, 5, 10, 20, 30, 40, 50, and 65 iterations.

see some smaller features evolving. The bottom row illustrate the design after 40, 50 and 65 iterations. During the late part of the optimization the trend of increasing the mouth diameter stops, in fact the mouth diameter decreases during these last 25 iterations.

Next, we study transmission efficient *low frequency* interfacial devices. Here, we use half-octave-wide frequency bands letting them start at different notes for optimization. Figures 4.16 and 4.17 show the resulting shapes for type 1 and type 2 parameterizations, respectively, and Figure 4.18 the corresponding reflection spectra. The resulting shapes illustrate that the interfacial device gets larger as the frequencies that are to be transmitted decreases. This trend is clear for both the convex (type 1) as well as the increasing (type 2) devices. The preference for smooth shapes when using the type 1 parameterization can be a particular advantage for higher frequencies, whereas it can be a liability for the lower frequencies; we obtained better transmission properties using the type 2 parameterization when optimizing in the difficult low-frequency region.

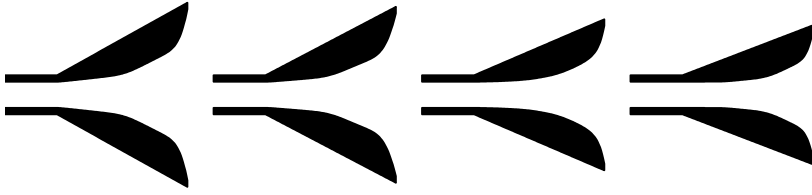


Figure 4.16: Shapes of interfacial devices of type 1 optimized for different frequency bands: $440 \cdot (2^{m/12}, \dots, 2^{(m+6)/12})$, from left: $m = -6$, $m = -3$, $m = 0$ and $m = 3$.

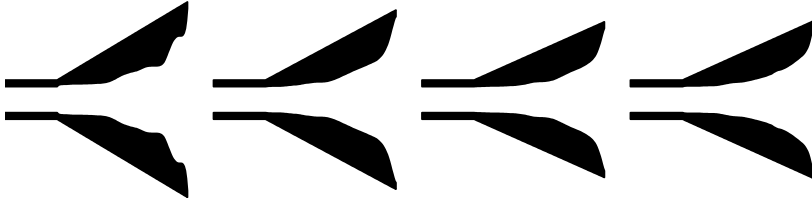


Figure 4.17: Shapes of interfacial devices of type 2 optimized for different frequency bands: $440 \cdot (2^{m/12}, \dots, 2^{(m+6)/12})$, from left: $m = -6$, $m = -3$, $m = 0$ and $m = 3$.

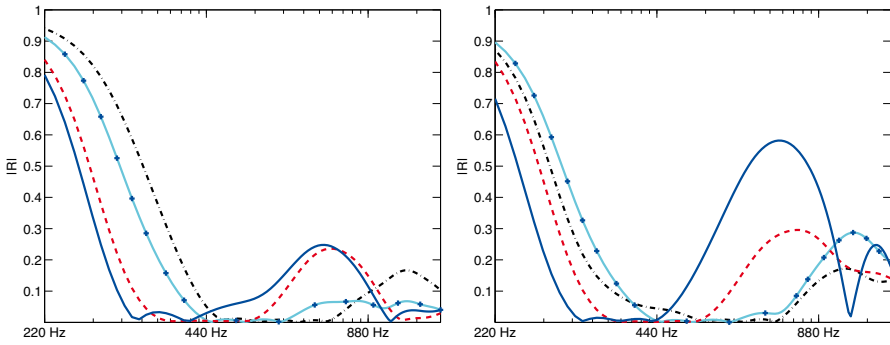


Figure 4.18: Reflection spectra for the shapes in Figures 4.16 (left diagram) and 4.17 (right diagram). optimized for frequency bands $440 \cdot (2^{m/12}, \dots, 2^{(m+6)/12})$, where $m = 3$ (dashed dotted), $m = 0$ (solid crossed), $m = -3$ (dashed) and $m = -6$ (solid).

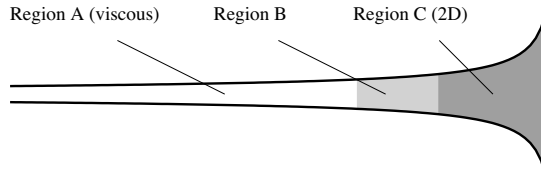


Figure 4.19: Partitioning of the instrument in domains. Region A and B are treated using the transmission line model, whereas region C is treated using a finite element method.

4.5 Paper IV

This paper presents how the shape of a brass instrument can be optimized with respect to its intonation. The instrument is modeled using a hybrid method between a one-dimensional transmission line analogy for the slowly flaring part of the instrument, and a finite element model for the rapidly flaring part. The bore of a typical brasswind instrument can be divided into three regions, as illustrated in Fig. 4.19. In the narrow and slowly flaring region A, viscous and thermal effects are considerable. In region C the horn has widened enough to make viscous effects small, but introduces two-dimensional effects. In the widening intermediate region B, neither viscous nor two-dimensional effects are pronounced. Therefore we use hybrid method, where region A and B are treated using the transmission line model, and region C is treated using the finite element method.

The hybridization principle of modeling is carried over into the optimization scheme. The optimization is carried out in a predictor-corrector scheme consisting of two consecutive steps. First, a design is made using the one dimensional model throughout the length of the instrument. Region C of the obtained profile is then re-optimized using the two-dimensional model.

The hybrid optimization scheme proceeds as follows

1. Specify the target peak impedance frequencies for the instrument
2. Perform optimization throughout the length of the instrument using the TL model to match the impedance peak frequencies of the instrument.
3. Find the starting point of region C.
4. Compute the input impedance spectrum for that point using the TL model.
5. Perform 2D optimization using the FEM model for horn flare in region C to match the target impedance from step 4.
6. Analyze the complete instrument using the hybrid TL+FEM model.

Let $\boldsymbol{\eta} \in \mathbb{R}^m$, denote a set of parameters defining the instrument shape. Diameters y_1, \dots, y_{N+1} and segment lengths L_1, \dots, L_N in Fig. 4.20 completely specify the geometry of the instrument in the case of the 1-D transmission

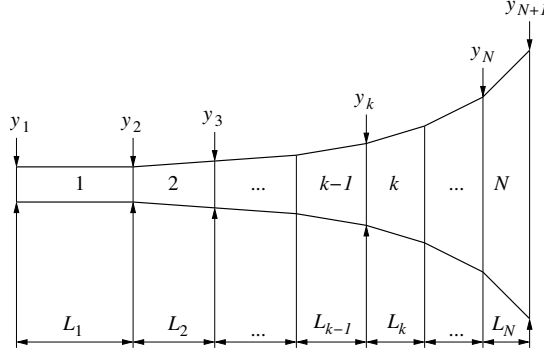


Figure 4.20: The horn approximated by a series of conical waveguide segments.

line model. The optimization in step 2 above minimizes the difference between the target frequencies and the frequencies of impedance peaks of the instrument. Let $Z_{\text{in}}(f, \boldsymbol{\eta})$ denote corresponding input impedance as a function of frequency f . Let f_i^d , $i = 1, \dots, n$ be the *desired* (real) resonance frequencies, and denote by f_i the *actual* i th zero of function $f \rightarrow \text{Im}(Z_{\text{in}}(f, \boldsymbol{\eta}))$. Our optimization problem can then be formulated

$$\min_{\boldsymbol{\eta}} F(\boldsymbol{\eta}) = \frac{1}{2} \sum_{i=1}^n (f_i - f_i^d)^2$$

subject to

$$\text{Im}(Z_{\text{in}}(f_i, \boldsymbol{\eta})) = 0, \quad i = 1, \dots, n.$$

The 1-D optimization step was carried out using design variables $\boldsymbol{\eta} = (L_1, \dots, L_N)$, with $\boldsymbol{\eta} \geq \mathbf{0}$, keeping a predefined set of increasing diameters fixed throughout the optimization. The resulting design is then guaranteed to be monotonically increasing.

The impedance spectrum Z_{1D} of the 1D optimized instrument, at the interface between region B and C, is calculated using the TL model. Then we use relation (4.8) to calculate the required reflection spectrum R_{1D} , which is used in the 2D optimization with the FEM model. We use a similar mathematical model as in Paper I. Assume now that equation (4.20) is solved for a particular value of the design variable $\boldsymbol{\eta}$ and at frequency ω_l . With an incoming wave of amplitude $A = 1$ generated at Γ_{in} , assumed to be placed at axial coordinate $z = 0$, the sound field in the entry can be written $p(r, z; \boldsymbol{\eta}; \omega_l) = \exp(-ikz) + R(\boldsymbol{\eta}; \omega_l) \exp(ikz)$, assuming an $\exp(i\omega t)$ dependence. The amplitude of the reflected wave at Γ_{in} will then be $R(\boldsymbol{\eta}; \omega_l) = p(r, 0; \boldsymbol{\eta}; \omega_l) - 1$, and the objective function is defined as

$$F(\boldsymbol{\eta}) = \frac{1}{2} \sum_l w_l \left| p(r, 0; \boldsymbol{\eta}; \omega_l) - 1 - R_{1D}(\omega_l) \right|^2. \quad (4.27)$$

Table 4.1: Intonation of resonances in musical cents for the different designs. The table shows the type of constraint used, and how well the resonances of the final horn corresponds with those from the one-dimensional design.

Variant	RMS difference (¢)	max difference (¢)
Bessel	33	103
Unc. $\epsilon = 10^{-2}$	6.4	17
Unc. $\epsilon = 10^{-4}$	3.2	10
Convex	4.4	8.9
Incr.	2.9	10

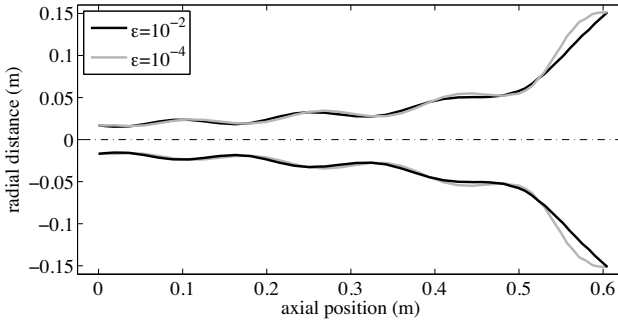


Figure 4.21: Shape of domain C of the horn with unconstrained optimization and two different degrees of regularization.

We carried out several numerical experiments for designing horn flare in region C with parameterization type 1 and 3. Figure 4.22 shows the shapes of region C, optimized with parameterization type 1 with convexity constraints $\eta \geq 0$. The horn flare consists of combinations of conical shapes. It should be noted that there are many design points in one conical elements. We also performed the same numerical experiments without convexity constraints with different amount of values 10^{-2} and 10^{-4} of regularization parameter. Figure 4.21 shows the optimized shapes. Figure 4.23 shows the shapes for instrument optimized with parameterization type 3 with increasing constraint $\eta \geq 0$. The shape can be approximately considered as combination of cylinders. There are many design points in these cylindrical elements as well. Finally, we optimized to find the Bessel horn that best match the impedance spectrum.

The complete optimized instrument is then analyzed with the TL+FEM hybrid model. The properties of optimized shapes are given in Table 4.1. In terms of performance of the instrument, the designs rank in the order increasing, unconstrained, convex, and Bessel, respectively. One would expect the unconstrained shape to outperform the increasing shape, since the

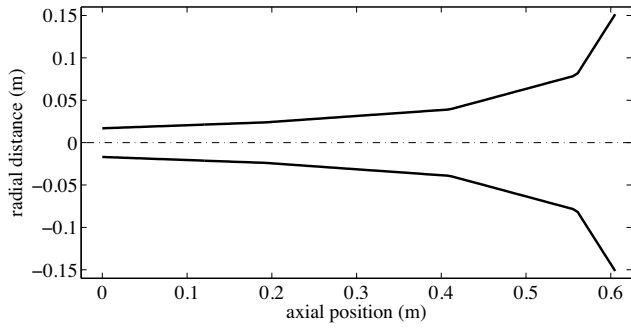


Figure 4.22: Shape of domain C of the horn with convexity constrained optimization and $\epsilon = 10^{-5}$. Note that there are many control points between the “corners”.

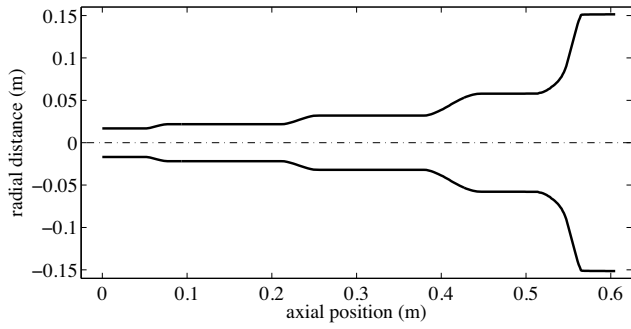


Figure 4.23: Shape of domain C of the horn with increasing constrained imposed. Note that there are many control points in each “straight section”.

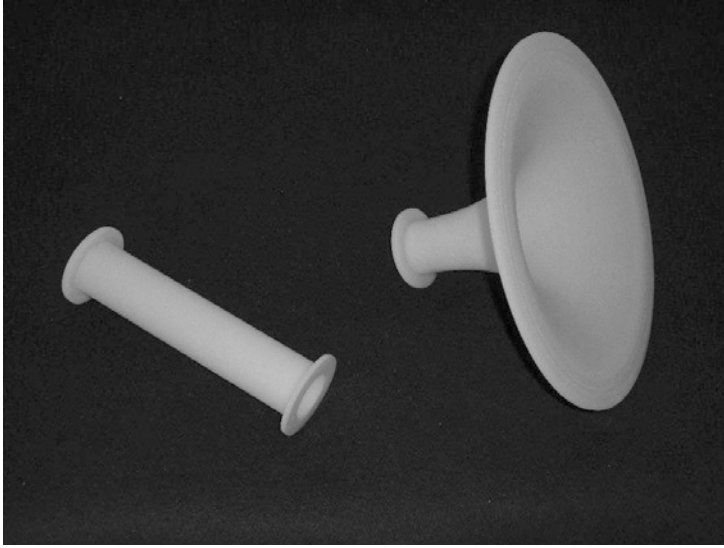


Figure 4.24: Horn prototype and connecting duct.

latter is in a subspace of the former, but the differences are small and a different choice of w_k might change the outcome. For any set of constraints, regularization improves smoothness at the expense of acoustical quality.

4.6 Paper V

The objective of this paper is to design a transmission efficient convex horn for a wide frequency band and to test the transmission properties experimentally. We use the algorithm described in paper I, to design an axisymmetric convex horn for the frequency band 1.6 kHz – 9.0 kHz.

A prototype of the optimized horn was built using stereolithography. Figure 4.24 shows a picture of the prototype and the connecting duct, which is used to feed the wave into the horn. The first author conducted measurements of the input acoustic impedance in anechoic chamber. Expression (4.8) shows that the input acoustic impedance for a perfectly transmitting horn, $R = 0$, should satisfy $Z_{\text{in}} = \rho c / s$.

Figures 4.25 and 4.26 compare the numerically predicted and the measured input acoustic impedances. It can be seen that the measured values agree reasonably well with the predicted optimal values up to about 7 kHz. The differences above 7 kHz are due to limitations in the measurement device.

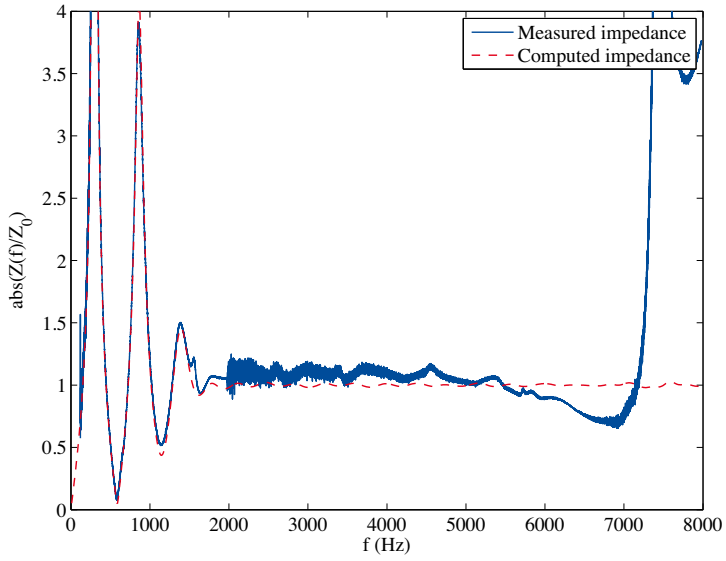


Figure 4.25: Computed and measured acoustic input impedance of the optimized horn: modulus.

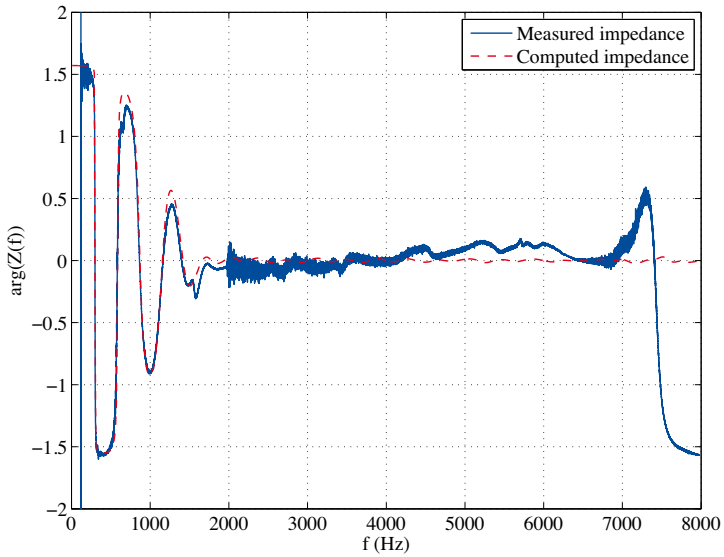


Figure 4.26: Computed and measured acoustic input impedance of the optimized horn: argument.

5. Summary in Swedish

Alltsedan datorn uppfanns har användandet av numeriska simuleringar ökat lavinartat. Under senare tid har det skett stora framsteg både vad gäller hård- och mjukvara för numeriska simuleringar. Det är numera möjligt att numeriskt simulera mycket komplexa system. Datorsimuleringar är nuförtiden ett standardverktyg vid teknisk projektering. Betydelsen av att skapa nya effektivare produkter växer i och med att ytterligare resursbegränsningar införs och formgivningsprocessen blir alltmer komplicerad. Forskare och ingenjörer fokuserar i allt större utsträckning på att hitta *optimala* lösningar till givna formgivnings- och konstruktionsproblem. Sökandet efter den ultimata designen kan utföras med hjälp av numeriska optimeringsmetoder.

I numerisk formoptimering används en *målfunktion* som kvantifierar en konstruktions prestanda. För att beräkna prestandan av en viss utformning löses en *tillståndsekvation*, vilken i denna avhandling kommer att vara en partiell differentialekvation. Optimeringsprocessen söker efter extremvärden av målfunktionen genom att successivt förändra utformningen.

Numeriska formoptimeringsmetoder kan delas upp i tre huvudgrupper: *storleksoptimering*, *randformoptimering* och *topologioptimering*. I storleksoptimering är de ingående delarna, men ej deras storlek, förutbestämda. Det som söks är exempelvis längden av balkar eller vilken plåttjocklek som skall användas. Randformoptimering använder sig av lokala randförskjutningar för att hitta den optimala utformningen. Vid dessa simuleringar används kroppsanpassade nät, något som ger hög noggrannhet i randbeskrivningen. Randformoptimering är således väl lämpat för problem där randens glatthet har stor betydelse, exempelvis för problem där gränsskikt uppkommer (såsom luftflöde kring en flygplansvinge). I topologioptimering görs inte några antaganden angående utformningens topologi. Designen växer fram under optimeringsprocessen och hål respektive fritt svävande delar kan träda fram och försvinna när som helst. Detta gör att metoden kan producera mycket komplicerade former. Topologioptimering används vanligtvis i den inledande konstruktionsfasen. Därefter används ofta randformoptimering och storleksoptimering för att ytterligare förfina resultatet. Ett aktuellt exempel är ett projekt vid Airbus UK Ltd. [32] där en flygplansvinges interna balkstruktur utformades enligt ovanstående strategi.

Det mänskliga örat är mycket känsligt för subtila ljudskillnader. Numeriska metoder för akustikberäkningar behöver därför kunna förutspå sådana skillnader. Det finns många väl använda numeriska metoder som kan analysera och beräkna transmissions- och spridningsegenskaper hos akustiska horn. De enklaste metoderna är endimensionella så kallade transmissionsledningsmodeller. För två- och tredimensionella problem används oftast finitaelement- och randelementmetoder. Överraskande nog verkar det i litteraturen finnas ytterst få försök att utforma akustiska horn med hjälp av numeriska simuleringar. Formoptimering har dock i några fall använts för att designa högtalarhorn [4, 22, 35, 50, 51] och bleckblåsinstrument [7, 29, 40, 46].

Denna avhandling behandlar numerisk formoptimering för akustiska vågutbredningsproblem och är baserad på fem artiklar vars innehåll beskrivs kort nedan.

Ett av huvudsyftena med Artikel I är att utveckla en robust randformoptimeringsalgoritm som kan användas för utformningen av akustiska horn. Vi använder denna algoritm för att formge plan- och cylinder-symmetriska horn med goda effektivitets- eller spridningsegenskaper. Det visar sig dock vara svårt att enbart med randformoptimering formge horn med hög effektivitet och jämn riktningsverkan. Därför använder vi i Artikel II oss samtidigt av topologi- och randformoptimering och formger en horn-lins kombination med hög effektivitet och stor spridningsvinkel för ett brett frekvensband.

I Artikel I och II är hornets längd och bredd förbestämda. I Artikel III specificerar vi hornets längd men inte dess mundiameter, vilket ger ytterligare frihet för nya utformningar. För att inte införa någon a priori information, låter vi optimeringen börja från en rak vågledare. De resulterande utformningarna är mycket transmissionseffektiva. Vidare antyder resultaten att det finns en naturlig övre gräns för hornets mundiameter.

Vi optimerar formen av bleckblåsinstrument i Artikel IV. Instrumenten modelleras med en hybridmetod. Vårt mål är att formge instrument med så bra intonationsegenskaper som möjligt. Optimeringsstrategin lyckas framställa ett antal oortodoxa men enkla former av klockstycken på instrument med goda intonationsegenskaper.

Slutligen testar vi experimentellt transmissionsegenskaperna för ett horn designat med metoden som utvecklats i Artikel I. Hornet är utformat för att ha ideal transmission i frekvensintervallet 1.6–9.0 kHz. Artikel V presenterar mätningar av den akustiska impedansen för detta horn.

6. Acknowledgment

I would like to express my heartfelt gratitude towards my advisor, Professor Martin Berggren, first for accepting me as a student and then for guiding me through all the phases of this thesis. Martin, you have been a very good friend and a mentor, and it is always enjoyable to work with you.

I sincerely thank my co-authors Eddie Wadbro, Daniel Noreland, and Pablo Seoane for their help and for many interesting discussions. Eddie and Malin, thanks for helping me to write the Swedish summary.

I am very grateful to Professor S. Ratnajeevan H. Hoole for all the motivations and inspirations since my undergraduate years. I extend my appreciation to Kandasamy Pirapaharan for his help during this period.

Swedish International Development Cooperation Agency (SIDA) is gratefully acknowledged for the financial support. I would also like to thank Richard Wait and University of Colombo School of Computing (UCSC) for coordinating the project.

Special thanks goes to all the members of the department of Information Technology of Uppsala University, for all the help and for the enjoyable environment. Thanks for many interesting discussions, seminars, courses, etc. I really enjoyed working here. Many thanks to Tom Smedsaas, Ulrika Andersson, and Carina Lindgren for their help during this period. I would like to thank the department of Computing Science, Umeå University for facilitating my visits. I thank to all Sri Lankan friends in Uppsala for making my stay feels like home.

I wish to pay my gratitude to all my teachers in the school and university days. I would like to thank the department of Electrical and Information Engineering of University of Ruhuna, Sri Lanka, for their help during the period.

I thank my mother and father for their help. I am indebted to you for your sacrifices and dedication throughout all these years. I am really grateful to my loving Erandi, for all the sacrifices made during these long years. Finally to Janiru, for giving me lot of motivation and happiness.

Bibliography

- [1] R. J. Alfredson. The propagation of sound in a circular duct of continuously varying cross-sectional area. *J. Sound Vibration*, 23(4):433–442, August 1972.
- [2] O. Amoignon. AESOP—a numerical platform for aerodynamic shape optimization. *Optim. Eng.*, 2009. DOI 10.1007/s11081-008-9078-7.
- [3] W. K. Anderson and D. L. Bonhaus. Airfoil design on unstructured grids for turbulent flows. *AIAA journal*, 37(2), 1999.
- [4] E. Bängtsson, D. Noreland, and M. Berggren. Shape optimization of an acoustic horn. *Comput. Methods Appl. Mech. Engrg.*, 192:1533–1571, 2003.
- [5] A. Bondeson, Y. Yang, and P. Weinerfelt. Shape optimization for radar cross sections by a gradient method. *Int. J. Numer. Meth. Engrg.*, 61:687–715, 2004.
- [6] D. Brackett, I. Ashcroft, and R. Hague. Multi-physics optimisation of 'brass' instruments—a new method to include structural and acoustical interactions. *Structural and Multidisciplinary Optimization*, 2009.
- [7] A. C. P. Braden, M. J. Newton, and D. M. Campbell. Trombone bore optimization based on input impedance targets. *J. Acoust. Soc. Am.*, 125:2404–2412, 2009.
- [8] H. Brauer and M. Ziolkowski. *Computer Engineering in Applied Electromagnetism*, chapter Shape Optimization with Adaptive Simulated Annealing and Genetic Algorithms, pages 25–30. Springer Netherlands, March 2005.
- [9] T. F. Coleman and Y. Li. An interior, trust region approach for nonlinear minimization subject to bounds. *SIAM J. Optim.*, 6:418–445, 1996.
- [10] D. Colton and R. Kress. *Integral Equation Methods in Scattering Theory*. John Wiley & Sons Inc., 1983.
- [11] H. Deguchi, M. Tsuji, and H. Shigesawa. Compact low-cross-polarization horn antennas with serpentine-shaped taper. *IEEE Trans. Antennas and Propagation*, 52(10):2510–2516, Oct 2004.
- [12] Y. Ding. Shape optimization of structures, a literature survey. *Comput. & Structures*, 24(6):985–1004, 1986.
- [13] B. Engquist and A. Majda. Absorbing boundary conditions for numerical simulation of waves. *Math. Comp.*, 31(139):629–651, 1977.

- [14] G. Galilei. *Mathematical discourses and demonstrations, relating to Two New Sciences*. New York: Macmillan, 1914. Translated to English by H. Crew and A. Salvio.
- [15] M. B. Gilse and N. A. Pierce. An introduction to the adjoint approach to design. *Flow Turbul. Combust.*, 65:393–415, 2000.
- [16] H. H. Goldstine. *A History of the Calculus of Variations from the Seventeenth Through the Nineteenth Century*. Springer-Verlag, 1980.
- [17] C. Granet, G. L. James, R. Bolton, and G. Moorey. A smooth-walled spline-profile horn as an alternative to the corrugated horn for wide band millimeter-wave applications. *IEEE Trans. Antennas and Propagation*, 52(3):848–854, March 2004.
- [18] M. D. Gunzburger. *Perspectives in Flow Control and Optimization*. SIAM, Philadelphia, USA, 2003.
- [19] J. Hadamard. Leçon sur le calcul des variations. *Gauthier-Villard*, 1910.
- [20] R. T. Haftka and R. V. Grandhi. Structural shape optimization—a survey. *Comput. Methods Appl. Mech. Engrg.*, 57:91–106, 1986.
- [21] E. Heikkola, T. Rossi, and J. Roivanen. Fast direct solution of the Helmholtz equation with a perfectly matched layer or an absorbing boundary condition. *Int. J. Numer. Meth. Engrg.*, 57(14):2007–2025, 2003.
- [22] D. J. Henwood. The boundary-element method and horn design. *J. Audio Eng. Soc.*, 41(6):485–496, June 1993.
- [23] Y. Hsu. A review of structural shape optimization. *Comput. & Structures*, 25(1):3–13, November 1994.
- [24] A. Jameson. Optimum aerodynamic design using CFD and control theory. *AIAA paper*, 95-1729, 1995.
- [25] A. Jameson. Computational aerodynamics for aircraft design. *Science*, 245(4916):361–371, 1989.
- [26] A. Jameson and J. J. Alonso. Automatic aerodynamic optimization on distributed memory architectures. *AIAA paper*, 96-0409, 1996.
- [27] A. Jameson, N. Pierce, and L. Martinelli. Optimum aerodynamic design using the navier–stokes equations. *Theoretical and Computational Fluid Dynamics*, 10:213–237, 1994.
- [28] A. Jameson and J. Reuther. Control theory based airfoil design using the euler equations. *AIAA paper*, 94-4272, 1994.
- [29] W. Kausel. Optimization of brasswind instruments and its application in bore reconstruction. *Journal of New Music Research*, 30:69–82, 2001.

- [30] L. E. Kinsler, A. R. Frey, A. B. Coppens, and J. V. Sanders. *Fundamentals of acoustics*. John Wiley & Sons, New York, fourth edition, 2000.
- [31] W. E. Kock and E.K. Harvey. Refracting sound waves. *The Journal of the Acoustical Society of America*, 21(5):471–481, 1949.
- [32] L. Krog, A. Tucker, and G. Rollema. Application of topology, sizing and shape optimization methods to optimal design of aircraft components. Technical report, Airbus UK Ltd., Altair Engineering Ltd., 2002.
- [33] J. Mackerle. Topology and shape optimization of structures using FEM and BEM: A bibliography(1999-2001). *Finite Elem. Anal. Des.*, 39(3):243–253, January 2003.
- [34] B. Mohammadi. and O. Pironneau. Shape optimization in fluid mechanics. *Annu Rev Fluid Mech*, 36:225–279, 2004.
- [35] R. C. Morgans, A. C. Zander, C. H. Hansen, and D. J. Murphy. EGO shape optimization of horn-loaded loudspeakers. *Optimization and Engineering*, 9(4):361–374, 2008.
- [36] K. Nadaraja and A. Jameson. A comparison of the continuous and discrete adjoint approach to automatic aerodynamic optimization. *AIAA paper*, 2000-0667, 2000.
- [37] K. Nadaraja and A. Jameson. Studies of the continuous and discrete adjoint approaches to viscous automatic aerodynamic shape optimization. *AIAA paper*, 2001-2530, 2001.
- [38] N. K. Niklova, R. Safian, E. A. Soliman, M. H. Bakr, and J. W. Badler. Accelerated gradient based optimization using adjoint sensitivities. *IEEE Trans. Antennas and Propagation*, 52(8):2147–2157, 2004.
- [39] J. Nocedal and S. J. Wright. *Numerical Optimization*. Springer Verlag, second edition, 2006.
- [40] D. Noreland. A gradient based optimisation algorithm for the design of brass-wind instruments. Technical Report 2003-033, Uppsala University, May 2003.
- [41] P. G. Petropoulos. On the termination of the perfectly matched layer with local absorbing boundary conditions. *Journal of Computational Physics*, 143(2):665–673, 1998.
- [42] O. Pironneau. On optimum design in fluid mechanics. *J. Fluid Mech.*, 64(1):97–110, 1974.
- [43] O. Pironneau. Optimal shape design by local boundary variations. *Lecture Notes in Mathematics*, 1740:343–384, 2000.
- [44] N. V. Queipo, R. T. Haftka, W. Shyy, T. Goel, R. Vaidyanathan, and P. K. Tucker. Surrogate-based analysis and optimization. *Progr Aero Sc*, 41:1–28, 2005.

- [45] J. A. Samareh. A survey of shape parameterization techniques. In *CEAS/AIAA/ICASE/NASA Langley International Forum on Aeroelasticity and Structural Dynamics*, pages 333–344, 1999.
- [46] R. A. Smith and G. J. Daniell. Systematic approach to the correction of intonation in wind instruments. *Nature*, 262:761–765, 1976.
- [47] E. Stein and K. Wiechmann. New insight into optimization and variational problems in the 17th century. *Engineering Computations*, 20(5/6):699–724, 2003.
- [48] K. Svanberg. The method of moving asymptotes—a new method for structural optimization. *Int. J. Numer. Meth. Engng.*, 24:359–373, 1987.
- [49] E. Wadbro. On the far-field properties of an acoustic horn. Technical Report 2006-042, Department of Information Technology, Uppsala University, 2006.
- [50] E. Wadbro and M. Berggren. Topology optimization of an acoustic horn. *Comput. Methods Appl. Mech. Engrg.*, 196:420–436, 2006.
- [51] E. Wadbro and M. Berggren. Topology optimization of wave transducers. In M. P. Bendsøe, N. Olhoff, and O. Sigmund, editors, *IUTAM Symposium on Topological Design Optimization of Structures, Machines and Materials*, pages 301–310. Springer, 2006.
- [52] D. Yang, Y. C. Chung, and R. Haupt. Genetic algorithm optimization of a multi-sectional corrugated conical horn antenna. *Microw. Opt. Tech. Lett*, 38(5):352–356, Sept 2003.
- [53] Y. Yang, T. Halleröd, D. Ericsson, A. Hellervik, A. Bondeson, and T. Rylander. Gradient optimization of microwave devices using continuum design sensitivities from the adjoint problem. *IEEE Trans. Magn.*, 41(5):1780–1783, 2005.

Acta Universitatis Upsaliensis

*Digital Comprehensive Summaries of Uppsala Dissertations
from the Faculty of Science and Technology 709*

Editor: The Dean of the Faculty of Science and Technology

A doctoral dissertation from the Faculty of Science and Technology, Uppsala University, is usually a summary of a number of papers. A few copies of the complete dissertation are kept at major Swedish research libraries, while the summary alone is distributed internationally through the series Digital Comprehensive Summaries of Uppsala Dissertations from the Faculty of Science and Technology. (Prior to January, 2005, the series was published under the title "Comprehensive Summaries of Uppsala Dissertations from the Faculty of Science and Technology".)

Distribution: publications.uu.se
urn:nbn:se:uu:diva-112549



ACTA
UNIVERSITATIS
UPSALIENSIS
UPPSALA
2010